ROSE/TN/2003-01

Microscopic and Electrical Properties of Clustered Divacancies in n-Type Silicon

M. Kuhnke
Department of Electronic and Computer Engineering,
Brunel University, Uxbridge, Middlesex UB8 3PH, United Kingdom
(Dated: January 27, 2003)

In crystalline silicon irradiated with high energy particles it is predicted that mainly clustered divacancies will be generated. A simulation method is described to calculate the potential energy distribution in the clusters and their electrical properties. A Gaussian distribution of divacancies is used. It is shown that the ratio $[VV(=)]/[VV(-)]$ depends on the number of divacancies in a cluster and on the cluster diameter. Therefore using the ratio $[VV(=)]/[VV(-)]$ from DLTS measurements on high resistivity n-type silicon and the average cluster diameter from TEM pictures together with simulated data the mean number of divacancies in a cluster can be estimated. The DLTS capture characteristics of the negative charge states of the divacancy $VV(-/=)$ and $VV(0/-)$ are described reasonably by the simulated capture characteristics. The results are discussed in relation to the build-up of an impurity-defect shell and annealing of the cluster damage.

I. INTRODUCTION

The radiation damage in n-type silicon after high energy particle irradiation is different in comparison to ^{60}Co γ-photon irradiation.[1] During irradiation of crystalline silicon with particles or γ-photons lattice atoms are displaced.[2] The threshold energy to displace a silicon atom is about 20 eV. An irradiation with ^{60}Co γ-photons is similar to an irradiation with electrons that have an energy of about 1 MeV. A homogeneous point defect distribution is produced, since the transferred kinetic energy to the host atoms is in the order of the displacement threshold energy. In contrast scattered heavy particles transfer much more kinetic energy to the host atoms. Silicon atoms with an energy more than 10 keV produce single displacements at the beginning of their stopping range and at the end a region with a high density of displacements. Silicon atoms with an energy of more than several 10 keV produce a tree-like collision cascade with terminal damage regions. The main portion of the energy is lost in the terminal damage regions. These regions form clusters of defects after relaxation. The threshold energy for cluster generation is estimated to be 300 eV.[3] Silicon atoms with an energy less than the threshold energy for cluster generation produce mostly single displacements. The size of a collision cascade region is in the order of the average stopping range of the primary recoiled silicon atom. The primary generated defects are silicon interstitials I and vacancies V. For particle irradiation where the stopping range is much longer than the sample thickness the damage comprising clusters and point defects is generated homogenously in the sample volume. In the case of heavy ion-implantation where the stopping range is much shorter than the sample thickness point defects are mainly produced beneath the sample surface and clusters in the highly damaged region at the end of the stopping range of the incident particle.

The composition of the collision cascades has been studied in Ref. 4. The hadronic interactions between the incident particle and the silicon nucleus are concerned. The TRIM code is employed to simulate the transport of ions in the silicon medium. If the kinetic energy is below the value of the displacement threshold energy, the recoiled silicon atoms or the fragments of silicon nuclei are stopped. Simulation data for 10 MeV protons, 23 GeV protons, 1 MeV neutrons and 200 MeV π^+-pions are presented. For the charged particles the homogeneous generation of single displacements is enhanced due to coulomb interaction. The thermally activated defect migration of the primary defects I and V and the formation of the intrinsic defects I_2, VV and V_3,...,V_6 and the impurity defects C_i, C_iC_s, C_iO_i, C_iC_sI, C_iO_iI, VP_s, VO_i, V_2O and V_3O is simulated. The initial concentration of the dopant phosphorus is $[P_s] = 1 \times 10^{12}$ cm^{-3}. The initial concentration of interstitial oxygen is either $[O_i] = 5 \times 10^{15}$ cm^{-3} or 5×10^{17} cm^{-3} and the initial concentration of substitutional carbon is $[C_s] = 1 \times 10^{16}$ cm^{-3}. A dependence of the defect kinetic on the particle type and energy and on the oxygen concentration is observed. However, the predictive power of such binary collision approximation (BCA) models including defect kinetics is limited, since many free parameters, e.g. the capture radii of defect reactions, are employed.[5]

In addition, the creation of strain and deformation fields is not taken into account and the partial dissipation of the transferred kinetic energy into thermal energy (phonons) is considered to be only due to energy transfers below the displacement threshold energy. In general, these two effects have a small influence on the energy deposition into displacement damage and ionization. Further on, the conversion of stored energy into thermal energy, as the electron-hole pairs caused by ionization recombine and as the crystal lattice structure in the dense displacement regions is partially restored by the rearrangement of larger intrinsic structural defect regions, is disregarded. After

the partial reconstruction of the lattice bond structure in the dense displacement regions, also known as heat-spike phase, the defect kinetics, e.g. the annihilation of Frenkel pairs $V + I \rightarrow \emptyset$, the generation of divacancies VV or other intrinsic defects and the diffusion of mobile intrinsic defects out of the cluster region, take place. Thus classical molecular-dynamics (MD) methods are used to simulate the displacement damage during the heat-spike phase, which has a duration of a few picoseconds. Otherwise, the main problem of MD methods is the choice of a good interatomic potential which describes the interactions in an energetic collision cascade far away from thermal equilibrium conditions suitable.[5]

In Ref. 6 the formation of collision cascades in a silicon crystal due to silicon recoils with an energy 0.4−10 keV has been studied in more detail with MD methods. The displacement damage which is created by silicon recoils with an energy more than 1 keV has the form of a small cascade. This cascade can be a subcascade of the aforementioned tree-like collision cascade. The number of displaced atoms is proportional to the energy loss due to nuclear scattering. The damage is separated into clusters of defects and isolated point defects in the vicinity of the clusters. An interstitial defect is defined as a Wigner-Seitz cell with more than one silicon atom and a vacancy defect as an empty Wigner-Seitz cell. Networks of defects are recognized as clusters. For silicon recoils with an energy 0.4−10 keV the number of defects in a cluster is mostly less than ten. Silicon recoils with an energy 2−10 keV generate additionally larger clusters with 10−70 defects. The number of defects in a cluster is not more than 90. The small clusters and the point defects comprise mainly interstitial defects. Vacancy defects prevail in the large clusters. The large clusters can be also interpreted as disordered regions. The thermally activated defect migration after the initial cascade generation and the formation of defect complexes is not simulated.

Deep level transient spectroscopy (DLTS) measurements suggest that divacancies VV are mainly formed in the cluster regions, but other unidentified defects seem to be hidden in the broadening of the signal $VV(-/0)$ after particle irradiation[1,3,7–10] — thus the peak in DLTS spectra is often designated $VV(-/0)$+?. The unidentified defects are assumed to be intrinsic defects generated in the cluster regions, but they have a much smaller generation rate than the divacancy. However, one have to add that only defects with energy levels in the band gap can be observed with the DLTS method.

Diffuse X-ray scattering (DXS) indicates that interstitial clusters are generated during ion-implantation.[11] These data put an upper limit of four defects on the vacancy and interstitial cluster size.

II. CLUSTERED DIVACANCIES

As mentioned in the previous section, the DLTS method is a useful technique to measure the concentrations of the various charge states of the divacancy.[7,9,12,13] The divacancy has four charge states $VV(=)$, $VV(-)$, $VV(0)$ and $VV(+)$. The positions of the acceptor levels $VV(=/-)$ and $VV(-/0)$ are in the upper half of the band gap and the position of the donor level $VV(0/+)$ is in the lower half of the band gap. For ^{60}Co γ-photon and 2 MeV electron irradiation the concentration ratio of the two negative charge states of the divacancy is $[VV(=)]/[VV(-)] \approx 1$ as expected for isolated divacancies.[1,13] After particle irradiation the ratio $[VV(=)]/[VV(-)]$ is smaller than one in n-type silicon. The ratio depends clearly on the particle type and energy and on the annealing state.[3,7,10]

It has already been proposed that only a fraction of the divacancies in a cluster is in the double negative charge state at low temperature due to compensation of free charge carriers in the cluster core.[14] A dependence of the ratio $[VV(=)]/[VV(-)]$ on the particle type and on the annealing state has also been reported in Ref. 13,15. For the first time, a model[13] has been proposed to explain the ratio $[VV(=)]/[VV(-)] < 1$ using the "locking" of the divacancy in a low-symmetry configuration (point group C_{2h}) at low temperature. Lattice strain and deformation associated with a highly damaged cluster region suppresses the reorientation of the divacancy. At high temperature the internal strain field does not prevent the reorientation and the enhanced-symmetry configuration (point group D_{3d}) occurs due to thermally activated configurational switching between low-symmetry configurations. The positions of the divacancy charge-state transitions in the band gap are assumed to be different for the low-symmetry and enhanced-symmetry configurations. It is not clear whether the theory of electronic bond switching[16] can be adapted to explain the experimental results in Ref. 13,15.

Further on, the speculation that defects which could also cause the broadening of the DLTS signal $VV(-/0)$ result in a reduction of the signal $VV(=/-)$ compared to the signal $VV(-/0)$ can be abandoned, since both signals $VV(=/-)$ and $VV(-/0)$ are broadened and the dependence of the full width at half maximum (FWHM) of the $VV(=/-)$ and $VV(-/0)$ peaks on the implantation temperature for 0.6 and 5.6 MeV ^{28}Si ions are described by the same function type in Fig. 9 of Ref. 15. This provides strong evidence of distorted divacancy centers. The energy levels of the divacancy in the cluster regions may have an exponential density distribution due to lattice compression.[10] Also the independence of the generation of $VV(-/0)$ levels per ion-induced vacancy[17] and a dependence of the generation of $VV(=/-)$ levels per ion-induced vacancy on the ion mass for implantation at $T = 295$ K in Fig. 7 of Ref. 15 support the assumption that the generation of cluster defects does not depend on the mass of the used ions and that another

effect is responsible for the reduction of the $VV(=/-)$ signal.

Capture measurements indicate that the capture rates of electrons into the neutral and negative charge states of the divacancy are not constant.[7] The capture rates are reduced for both processes $VV(0/-)$ and $VV(-/=)$.

No simulations have so far been performed to explain the particle dependence of the ratio $[VV(=)]/[VV(-)]$ and the reduced capture rates of the processes $VV(0/-)$ and $VV(-/=)$.

III. MOBILITY OF INTERSTITIAL CLUSTERS

The properties of interstitial clusters are not so well investigated as the properties of the divacancy.

In Ref. 18 *ab initio* molecular-dynamics simulations have shown that in absence of minority charge carriers the interstitial clusters $I_3^{(b)}$ and I_4 have each one stable (not diffusing on the time scale $\sim$10 ps at $T = 1000$ K) configuration. However, silicon di-interstitials I_2, which exist in only one configuration, and another configuration of $I_3^{(a)}$ — the most stable one — are rapidly diffusing at $T = 77$ K or 1000 K. Also, the most probable configuration of I is stable at these temperatures. Otherwise, silicon interstitials I diffuse extremely fast, when minority charge carriers are present.

These results on silicon interstitial and di-interstitial mobilities contradict the results interpreted from diffuse X-ray scattering investigations, which assume that the thermally activated motion of I commences at $T \approx 150$ K and that the precipitate I_2 is immobile below room temperature.[19] The athermal motion of I below $T \approx 150$ K may be induced by electronic excitation.

In Ref. 20 the building blocks of silicon interstitial precipitation are thought to be the extremely mobile interstitial clusters I_2 and I_3 which are locally formed in regions with a high density of silicon interstitials I. The energy gains of the reactions $I_3 + I_3 \rightarrow I_6$, $I_3 + I_6 \rightarrow I_9$ and $I_2 + I_6 \rightarrow I_8$ are over 2.5 eV.

IV. CLUSTER AND DEFECT KINETICS

In situ Transmission Electron Microscopy (TEM) can be used to determine the diameter of clusters.[21,22] During heavy ion bombardment the formation of dense collision cascades with subclusters is observed with extinction TEM. The average diameter of a subcluster (a cluster in a dense collision cascade) created during heavy ion-implantation is in the range from 2.5 to 5 nm.[21] The contrast and density of the clusters generated during implantation with silicon ions of a few 10 keV is not high enough to be visible, but it is reasonable to assume that the clusters generated during high energy particle irradiation have likely the same size as the subclusters. A time evolution of the cluster damage is also observed.[22] The time scale is in the order of ten seconds at room temperature.

A model, that describes the static electrical properties of a spherical cluster, can be found in Ref. 23. Microscopic and electrical properties of the cluster damage in n-type silicon obtained from analyzing the charge carrier removal rate after neutron irradiation have been compiled in Ref. 24. The density distribution of divacancies in a clusters is given by a Gaussian distribution. Moreover, ionization during irradiation can alter the population of the defect charge states and hence the electric field distribution within the clusters. It has been suggested that during cluster formation the electric field distribution within the clusters plays an important role.[25] During this phase of formation it is thought that the cluster regions contain only vacancies and divacancies. The silicon interstitials have already diffused out of the primary damage regions.

Further on, a dependence of the number of divacancies in a cluster on the neutron flux has been suggested in Ref. 26. This effect is attributed to an increase in the annihilation rate of divacancies located in the cluster regions with diluted interstitial atoms on increase in the neutron flux. Also, it has been proposed that the cluster damage influence the migration of point defects generated in the crystal matrix, in which the clusters are embedded, and thus an impurity-defect shell builds up in the surroundings of the clusters.[27]

Furthermore, the annealing characteristic of divacancies concentrated in the clusters is assumed to be different from the annealing characteristic of single divacancies due to the movement of interstitial atoms liberated from the impurity-defect envelope towards the cluster core.[28] However, a combination of various effects can cause the exponential or logarithmical decrease of the concentrations of cluster defects during isothermal annealing at a moderate temperature $T = 60$ °C.[10]

Recent experimental results indicate that interstitial carbon atoms C_i generated by the exchange reaction $I + C_s \rightarrow C_i$ are attracted to the cluster regions and their final migration volume is constricted in the environment of the clusters.[3,7,29] The impurity defect formation, $C_i + C_s \rightarrow C_iC_s$, $C_i + O_i \rightarrow C_iO_i$ and $C_i + VV \rightarrow C_s + V$, takes place in the cluster environment and at the cluster periphery, but the defect kinetics are still affected by the impurity content of oxygen and carbon. The interaction between a cluster and a point defect C_i is due to strain and deformation fields.[30]

An attractive interaction between vacancies over a few lattice constants due to lattice deformations has been discussed in Ref. 31. However, the migration of single vacancies V outside the cluster regions seem to be not affected by strain and deformation fields and hence no aggregation of the impurity defect VO_i in the neighborhood of the clusters occurs. One suggests that during neutron irradiation the defect VO_i and other vacancy-oxygen complexes V_nO are formed within the tree-like collision cascade regions and the surrounding volume, because the displacement damage is almost created in the collision cascade regions and the mobile vacancies are captured at the nearby interstitial oxygen O_i sites.[7]

In summary, the microscopic and electrical properties of cluster damage are elusive and not well understood.

V. SIMULATION METHOD

A. Thermal equilibrium conditions

The majority charge carriers in the materials investigated are electrons. Under thermal equilibrium conditions the electronic band structure is bent due to charged clusters.[32] The band structure has been calculated for the special case of a Gaussian distribution of divacancies in the clusters and a homogeneous distribution of shallow dopant impurities in the bulk. The contribution of other unidentified defects in the cluster regions to the charge density can be neglected, since their concentrations are small.[8,10] In the regions surrounding the negatively charged clusters the contribution of charged impurity defects to the positive space charge is neglected, since their concentrations are assumed to be much smaller than the dopant concentration after low fluence irradiations used for the DLTS studies. The density distribution of divacancies VV is

$$n_{VV}(r) = \frac{M}{\pi^{3/2}\, L_0^3} \cdot \exp\left(-\frac{r^2}{L_0^2}\right) \tag{1}$$

where M is the number of divacancies in a cluster, L_0 the characteristic width of the Gaussian distribution and r the radius from the cluster center. A Gaussian distribution is thought to be a good approximation of the real distribution profile assuming the initial cluster is a hot spot and during the cool-down phase the diffusion of divacancies occurs. Further on, one simplifies that the clusters are distributed homogeneously in the sample volume and that in a sphere with the radius

$$r_{max} = \sqrt[3]{\frac{3 \cdot M}{4\pi \cdot g(VV) \cdot \Phi_{eq}}} \tag{2}$$

in which a cluster is centered the condition of charge neutrality is valid. The radius r_{max} is obtained from a model which lines up the clusters in one dimension. Actually, the radius r_{max} depends on the introduction rate of divacancies $g(VV)$ and the equivalent fluence Φ_{eq}. The introduction rate is the defect concentration divided by the equivalent fluence or the generation of defect centers in an 1 cm^3 volume element, which exposes an 1 cm^2 cross-section perpendicular to the particle beam, per incident particle. The equivalent fluence is used to normalize between different particle sources.[8,33] The population of the charge states of the divacancy depends on the free charge carrier concentrations or the distance of the Fermi level from the conduction band edge. The bending of the electronic band structure alters the distance of the Fermi level from the conduction band edge. In the cluster center the potential energy is maximal and is non-zero at the boundary of the sphere with the radius r_{max}. The distribution of the potential energy is spherically symmetrical, since the Gaussian distribution depends only on the radius r. The occupancies of the neutral, single and double negative charge states under thermal equilibrium conditions are taken from Ref. 34. The charge density, which depends on the concentrations of ionized donor atoms, electrons, single and double negatively charged divacancies, at the radius r is

$$\rho(r) = q_0 \cdot \left[N_D - n - n_{VV}(r) \cdot \left(F^- + 2 \cdot F^=\right)\right] \tag{3}$$

$$n = n_0 \cdot \exp\left(-\frac{\psi(r)}{k_B T}\right) \tag{4}$$

$$\begin{aligned} F^- &= \frac{f_1}{1 + f_1 + f_1 \cdot f_2} \\ F^= &= \frac{1}{1 + f_1 + f_1 \cdot f_2} \\ F^0 &= \frac{f_1 \cdot f_2}{1 + f_1 + f_1 \cdot f_2} \end{aligned} \tag{5}$$

$$f_1 = \frac{N_C}{n_0} \cdot \exp\left(-\frac{\Delta E_1 - \psi(r)}{k_B T}\right)$$
$$f_2 = \frac{N_C}{n_0} \cdot \exp\left(-\frac{\Delta E_2 - \psi(r)}{k_B T}\right) \quad (6)$$

where $\psi(r)$ is the increase of the distance of the Fermi level from the conduction band edge (band bending energy), q_0 the electronic charge, N_C the effective density of conduction band states, n the free electron concentration that depends on the band bending energy $\psi(r)$ and n_0 the free electron concentration without divacancy clusters and hence with no band bending. The ionization energies of the transitions $VV(=/-)$ and $VV(-/0)$ are $\Delta E_1 = 0.25$ eV and $\Delta E_2 = 0.42$ eV.[7] The temperature dependence of the effective density of states is $N_C = 2.86 \times 10^{19}$ cm^{-3} $(T/300\text{K})^{1.58}$.[35] It is more convenient for the computation to express the densities in units of N_D, the energies in units of $k_B T$ and the lengths in units of the Debye length $L_D = \sqrt{\varepsilon_s \, k_B T/(q_0^2 \, N_D)}$. Because the concentration of defects outside the clusters is much smaller than the shallow dopant concentration, the free electron concentration without divacancy clusters is $n_0 = N_D$.

The spherically symmetrical charge distribution is described by a multi-shell approach. The charge density in each shell is homogeneous. The difference between the radii of two successive spherical surfaces is constant. The number of shells used is 10 000 or 50 000. Applying the Gaussian theorem the band bending energy at each spherical surface is iteratively computed with

$$\psi(r_{n+1}) = \frac{q_0 \cdot \rho(r_{n+1})}{6\,\varepsilon_s}\left(r_{n+1}^2 + 2\frac{r_n^3}{r_{n+1}} - 3\,r_n^2\right) - q_0 \cdot E(r_n) \cdot \left(\frac{r_n^2}{r_{n+1}} - r_n\right) + \psi(r_n) \quad (7)$$

$$E(r_n) = \frac{1}{3\,\varepsilon_s} \cdot \frac{1}{r_n^2} \sum_{i=1}^{n} \rho(r_i) \cdot (r_i^3 - r_{i-1}^3) \quad (8)$$

where ε_s is the permittivity of the semiconductor. In the simulation the electric field strength used unit is $E_D = (q_0 \, N_D \, L_D)/\varepsilon_s$. The starting radius is $r_0 = 0$. The electric field is zero at $r_0 = 0$. For a start value $\psi(r_0)$ the charge density $\rho(r_1)$ is calculated with Eq. (3). The band bending energy ψ and the electric field E at the radius r_1 is calculated with Eqs. (7) and (8). With $\psi(r_1)$ the charge density $\rho(r_2)$ is calculated and etc. The start value $\psi(r_0)$ is varied to fulfil charge neutrality

$$\frac{1}{q_0} \cdot \sum_i \rho(r_i) \cdot (r_i^3 - r_{i-1}^3) = 0 \; . \quad (9)$$

The algorithm is repeated until the evaluation of Eq. (9) is $\epsilon < 10^{-6}$.

B. Non equilibrium conditions

The rate equations which describe the time dependence of the occupancies of the charge states $VV(0)$, $VV(-)$ and $VV(=)$ are

$$\frac{dF^=}{dt} = v_{th,n} \cdot \sigma_1 \cdot (n\,F^- - n_1\,F^=) \quad (10)$$

$$\frac{dF^0}{dt} = v_{th,n} \cdot \sigma_2 \cdot (n_2\,F^- - n\,F^0) \quad (11)$$

$$F^0 + F^- + F^= = 1 \quad (12)$$

$$v_{th,n} = \sqrt{\frac{8 \cdot k_B T}{\pi \cdot m^*_{th,n}}} \quad (13)$$

$$\begin{aligned} n &= n_0 \cdot \exp\left(-\frac{\psi(r)}{k_B T}\right) \\ n_1 &= n_0 \cdot \exp\left(-\frac{\Delta E_1 - E_F}{k_B T}\right) \\ n_2 &= n_0 \cdot \exp\left(-\frac{\Delta E_2 - E_F}{k_B T}\right) \end{aligned} \tag{14}$$

$$E_F = k_B T \cdot \ln\left(\frac{N_C}{n_0}\right) \tag{15}$$

where $m_{th,n} = 0.27\ m_e$ is the effective thermal mass,[35] $\sigma_1 = 5 \times 10^{-15}$ cm^2 and $\sigma_2 = 3 \times 10^{-15}$ cm^2 the capture cross-sections of the transitions $VV(=/-)$ and $VV(-/0)$.[7] For the calculation of the Fermi level E_F the above-mentioned temperature dependence of the effective density of states N_C is regarded.[35]

However, the analytical solution of the coupled differential equations is a complicated expression and the simple numerical technique of multiplying the rate equations with a finite element Δt works only for very small time steps, especially for the capture process $VV(0/-)$. If the time steps are too large, the solution suddenly diverges at a certain time point. Therefore, the application of this technique is very time consuming. Otherwise, the change in the population of the charge state $VV(-)$ due to electron emission is negligible at $T = 125$ K — the temperature at which the capture characteristic of the process $VV(-/=)$ is measured — and the occupancy of the charge state $VV(0)$ is approximately zero. Thus the coupling is weak and only Eq. (10) together with the constraint $F^- + F^= = 1$ is employed to calculate the capture characteristic $VV(-/=)$ at $T = 125$ K. Moreover, the emission rate of electrons from the charge state $VV(=)$ is much higher than the capture rate of electrons into the charge state $VV(-)$ at $T = 200$ K — the temperature at which the capture characteristic of the process $VV(0/-)$ is measured. Therefore, the occupancy of the charge state $VV(=)$ is almost zero and does not change. Hence Eq. (11) together with the constraint $F^0 + F^- = 1$ is employed to calculate the capture characteristic $VV(0/-)$ at $T = 200$ K. For both temperatures $T = 125$ K and 200 K the weak coupling between the two differential equations is additionally confirmed by a comparison of simulated capture characteristics regarding all three charge states $VV(0)$, $VV(-)$ and $VV(=)$ with ones regarding only the two charge states $VV(-)$ and $VV(=)$ or $VV(0)$ and $VV(-)$. No deviation is observed.

Each differential equation has been solved analytically to avoid errors due to the simple technique of multiplying the rate equation with a finite element Δt. All divacancies are in the charge state $VV(-)$ at the beginning of the capture process $VV(-/=)$ and all divacancies are in the charge state $VV(0)$ at the beginning of the capture process $VV(0/-)$. The band bending energy distribution is calculated with the known occupancies of the different charge states. The value of the band bending energy in the cluster center is varied to fulfil charge neutrality. For further details see previous section. A smaller epsilon parameter $\epsilon < 10^{-9}$ is necessary to stabilize the algorithm. Once the distribution of free electrons is obtained, the change in the occupancies after a time step Δt is calculated with the analytical solution of the proper differential equation. Again the band bending energy distribution is computed and with the new electron distribution the change in the occupancies after another time step Δt is obtained. The initial time steps are about one order of magnitude larger than the dielectric time constant

$$\tau_{dielec} = \frac{\varepsilon_s}{q_0 \cdot n_0 \cdot \mu_n} \tag{16}$$

where μ_n is the mobility of electrons. The temperature dependence of the electron mobility is $\mu_n = 1411$ cm^2/Vs $(T/300\text{K})^{-2.133}$.[36] The dielectric time constant is the relaxation time constant for a small local disturbance of the majority charge carrier concentration from equilibrium conditions.[38] The width of the time steps increases logarithmically. The division of a decade into 50 or 100 steps is sufficient. The algorithm is broken for the capture process $VV(-/=)$, if the concentration $[VV(=)]$ starts to decrease, and for the capture process $VV(0/-)$, if the concentration $[VV(-)] + [VV(=)]$ starts to decrease, or simply, if the new calculated band bending energy distribution does not change. In the case where none of the above conditions apply, the algorithm is halted at a certain time point to avoid numerical errors and ensuing processor failure. The band bending energy distribution of the steady state coincides with the one obtained under thermal equilibrium conditions. This confirms the reliability of the time evolution of the charge state populations.

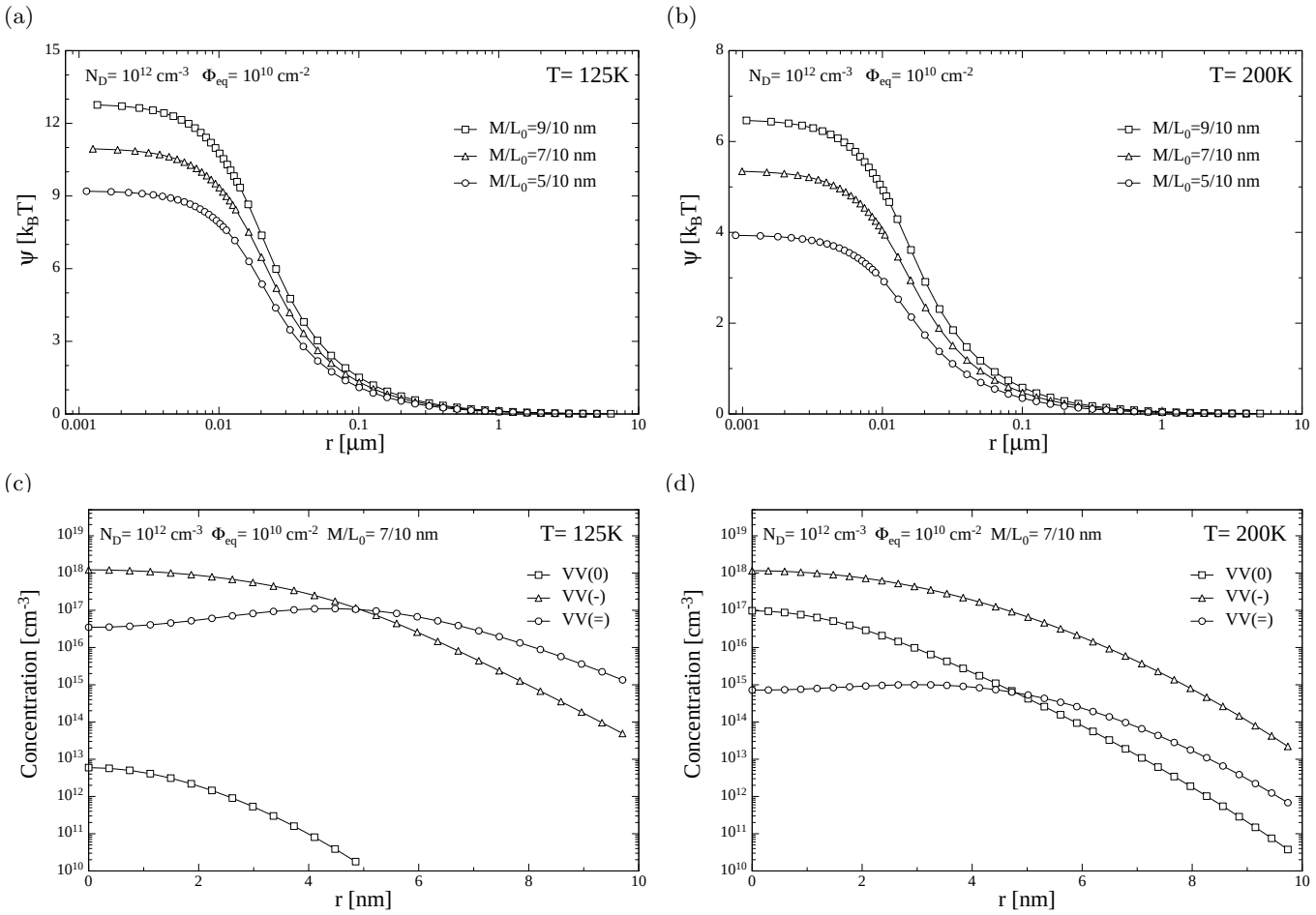

FIG. 1: The distributions of the band bending energy for a Gaussian distribution of divacancies (a,b) and the concentrations of the negative and neutral charge states of the divacancy (c,d) at two different temperature $T = 125$ K and 200 K have been simulated.

VI. RESULTS

A. Concentration Ratios

The concentration of the charge state $VV(=)$ is measured at $T \approx 125$ K and the concentration of the charge state $VV(-)$ at $T \approx 200$ K with the DLTS method.[3,7,8] In Fig. 1 simulation results are shown. For the temperatures $T = 125$ K and 200 K the band bending energy distributions and the concentrations $[VV(0)]$, $[VV(-)]$ and $[VV(=)]$ have been calculated. The number of divacancies in a cluster is $M = \{5, 7, 9\}$ and the width of the Gaussian distribution is $L_0 = 10$ nm. The temperature dependence of the band bending energy distribution and of the concentrations of the three charge states is obvious. The amount of band bending is greater at $T = 125$ K than at $T = 200$ K. At the lower temperature the divacancies in the cluster core are almost in the charge state $VV(-)$ and in the outer region in the charge state $VV(=)$. At the higher temperature the main portion of divacancies is in the charge state $VV(-)$. Therefore, the experimental result $[VV(=)]/[VV(-)] < 1$ is consistent with the theory. Simulations with various values of M and L_0 have been performed. The introduction rate of divacancies is $g(VV(-)) = 1.33$ cm^{-1} which models the experimental data well.[3,7] In Table I the other simulation parameters are listed. In Fig. 2 the thirty-six data points are plotted. A dependence on the shallow dopant concentration N_D is revealed. The dependence on the equivalent fluence Φ_{eq} is less than 4.5%. The concentration ratio $[VV(=)]/[VV(-)]$ for each dopant concentration has a coarse linear dependence on the line density M/L_0. This is an empirically found law and only valid for the employed values of M, L_0 and Φ_{eq}. The regression lines are $[VV(=)]/[VV(-)] = 0.976 - 0.817\,\mathrm{nm} \cdot (M/L_0)$ for $N_D = 10^{12}$ cm^{-3} and $[VV(=)]/[VV(-)] = 1.25 - 0.933\,\mathrm{nm} \cdot (M/L_0)$ for $N_D = 10^{13}$ cm^{-3}. For a crude estimation of the number of divacancies in a cluster an eventual particle dependence of the cluster diameter is disregarded. Using

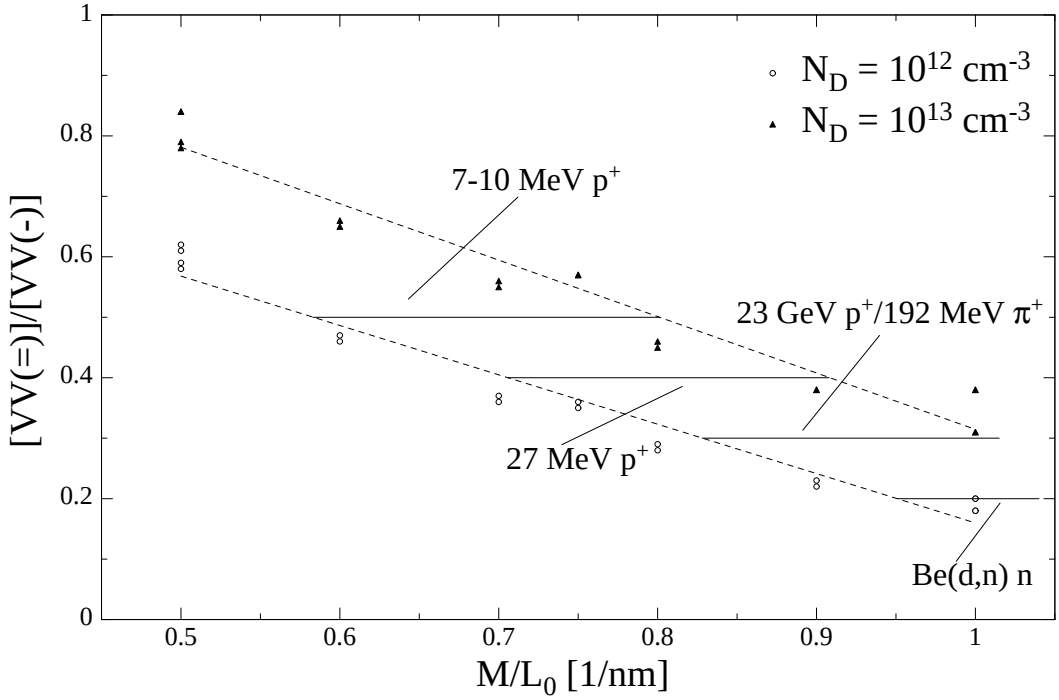

FIG. 2: The dependence of the concentration ratio $[VV(=)]/[VV(-)]$ on the line density M/L_0 for two dopant concentrations N_D has been calculated (open and solid symbols). The experimental values of $[VV(=)]/[VV(-)]$ for different particles are indicated by horizontal solid lines. Also the linear regressions of the data points are drawn (dashed lines). For further details see Tables I and II.

TABLE I: The parameters for which the simulation has been performed are listed.

N_D [cm^{-3}]	Φ_{eq} [cm^{-2}]	L_0 [nm]	M
10^{12}	10^{10}, 10^{11}	5	3, 4, 5
		10	5, 7, 9
		100	50, 75, 100
10^{13}	10^{11}, 10^{12}	5	3, 4, 5
		10	5, 7, 9
		100	50, 75, 100

$L_0 = 10$ nm estimated from TEM pictures[21] for the dimension of a cluster and the ratio $[VV(=)]/[VV(-)]$ obtained from DLTS spectra,[3,7] the number of divacancies in a cluster can be calculated with the regression parameters. One notes the chosen L_0 is by a factor 4−8 too large in comparison to the experimental data obtained from heavy ion-implantation.[21] However, the large cluster diameter may be justified, since firstly, the defect density in the outer cluster part is marginal and might be not observable with TEM, and secondly, the clusters contain only a few divacancies for $L_0 < 5$ nm, e.g. for $M = 4$, $L_0 = 5$ nm, $N_D = 10^{12}$ cm^{-3} and $\Phi_{eq} = 10^{10}$ cm^{-2} it is $[VV(=)/VV(-)] = 0.28$. In Table II the particle dependence of the number of divacancies in a cluster together with the experimental data are

TABLE II: The particle dependence of the number of divacancies in a cluster estimated from the experimental and simulation results are listed. The mean energy of the Be(d,n) neutrons is 5.3 MeV. The introduction rate $g(VV(-))$ and the ratio $[VV(=)]/[VV(-)]$ refer to an annealing state reached after heating for 80 min at 60 °C.

Particle type	$g(VV(-))$ [cm^{-1}]	$[VV(=)]/[VV(-)]$	L_0 [nm]	M	$n_{VV,center}$ [cm^{-3}]
p^+ 7-10 MeV	1.31	≈ 0.5	10	6−8	1.2×10^{18}
p^+ 27 MeV	1.26	≈ 0.4	10	7−9	1.4×10^{18}
p^+ 23 GeV/π^+ 192 MeV	1.32	≈ 0.3	10	8−10	1.6×10^{18}
n Be(d,n)	1.30	≈ 0.2	10	10−11	1.9×10^{18}

given.

The concentration of divacancies in the cluster center is in the range from 1.2×10^{18} cm^{-3} to 1.9×10^{18} cm^{-3} and hence inter-center-charge-transfer occurs between the divacancies in the clusters.[39] At low temperature $T = 125$ K the charge states $VV(-)$ and $VV(=)$ are populated. The charge exchange process $VV(-)+VV(=) \rightarrow VV(=)+VV(-)$ is symmetrical and neither of the occupancies of both charge states is changed. Otherwise, the charge exchange process $VV(-) + VV(-) \rightarrow VV(0) + VV(=)$ decreases the population of $VV(-)$ and increases the population of $VV(0)$ and $VV(=)$. At high temperature $T = 200$ K the population of the charge state $VV(-)$ may be slightly enhanced due to the charge exchange process $VV(0) + VV(0) \rightarrow VV(+) + VV(-)$, but again the charge exchange process $VV(-) + VV(-) \rightarrow VV(0) + VV(=)$ occurs. Altogether, the changes in the occupancies due to inter-center-charge-transfer is thought to be small under thermal equilibrium conditions.

The experimental observation of the increase in the concentration ratio $[VV(=)]/[VV(-)]$ during annealing[7] can be explained with a decrease in the divacancy concentration in the clusters. However, the dependence of $[VV(=)]/[VV(-)]$ (and also of $[VV(-)]/[VV]$) on the shallow dopant concentration N_D illustrated by the simulations is not consistent with the DLTS results. The measured ratio $[VV(=)]/[VV(-)]$ depends not on N_D in the range from 7×10^{11} cm^{-3} to 4×10^{13} cm^{-3}. However, after reactor neutron irradiation, which is assumed to generate very dense clusters, a dependence for high resistivity n-type silicon (N_D=7×10^{11} cm^{-3}) seem to emerge.[40] Also the introduction rate $g(VV(-))$ is reduced in this material after 23 GeV proton and reactor neutron irradiation compared to silicon material with a lower resistivity. Thus the experimental accuracy of the defect concentration determination from the DLTS spectra may obscure the N_D dependence, since the effect seen in the simulation is not very large. The experimental uncertainty is estimated to be roughly 20%.[7]

B. Capture Characteristics

In Fig. 3 the simulated and measured capture characteristics of the processes $VV(-/=)$ and $VV(0/-)$ are shown. In Figs. 3a and 3b the simulated capture characteristics with the parameters $M = 9$ and $L_0 = 10$ nm for the dopant concentrations $N_D = 10^{12}$ and $10^{13}\,\mathrm{cm}^{-3}$ are depicted. In Fig. 3a the shape of the capture characteristic $VV(-/=)$ depends on the dopant concentration N_D. In Fig. 3b the capture characteristic $VV(0/-)$ with the larger capture rate ($N_D = 10^{13}\,\mathrm{cm}^{-3}$) is shifted on the time scale with $\log(N_D/10^{12}\ \mathrm{cm}^{-3}) = 1$ and the two capture characteristics nearly superimpose. The capture process for a single defect is given in Ref. 7,41 and a commonly used approach is

$$\frac{|\Delta C|}{C_R} = \frac{N_T}{2 \cdot N_D} \left[1 - \exp\left(-\frac{t}{\tau_c}\right)\right] \tag{17}$$

$$\tau_c = \frac{1}{v_{th,n} \cdot \sigma_c \cdot n} \tag{18}$$

where ΔC is the amplitude of the capacitance transient, C_R the capacitance of the reverse biased p^+n junction, N_T the defect concentration, $v_{th,n}$ the thermal velocity, σ_c the capture cross-section, n the electron concentration and t the time. Therefore, a change in the electron concentration from n to $n' = n + \Delta n$ results into a shift on the logarithmic time scale $\log(n/n')$. In conclusion the capture process of clustered divacancies $VV(0/-)$ still depends on the free charge carrier concentration in the same way as the capture process of single divacancies with a constant capture rate. This feature is not observed for the other capture process of clustered divacancies $VV(-/=)$.

In Figs. 3c and 3d the capture characteristics measured in various samples after particle irradiation together with simulations are shown. In Table III the samples are described in detail. In Fig. 3c the capture characteristics $VV(-/=)$ are depicted. A dependence on the particle type and energy and on the annealing state is seen. The samples IIKA18 and II02A7 were annealed for longer periods. Thus the radiation damage is in the final stable annealing state. The ratios $[VV(=)]/[VV(-)]$ are nearly identical. Also the capture characteristics nearly coincide. Therefore, it is speculated that the cluster damage created during irradiation with Be(d,n) neutrons and 192 MeV π^+-pions is not very distinctive. The mean energy of the Be(d,n) neutrons is 5.3 MeV. The cluster damage in the samples W33402 and P50323 is also annealed to about the same state, but the ratios $[VV(=)]/[VV(-)]$ are different and the capture characteristics do not coincide. Hence the cluster damage generated by 10 MeV protons and reactor neutrons is distinctive. Further on, the capture measurements indicate that after long term annealing the cluster damage will not be in the same state unlike Be(d,n) neutron and 192 MeV π^+-pion irradiations. A detailed study of the particle dependence and annealing behavior of the capture characteristic $VV(-/=)$ is needed for better understanding of the cluster damage. The measured capture characteristics exhibit also a large deviation from the capture characteristic with a constant capture rate ($\tau_c = 200$ μs). In Fig. 3c the simulated capture characteristics, that describe reasonably the experimental data, are included. The parameters are $M = \{5, 9\}$ and $L_0 = 10$ nm. The

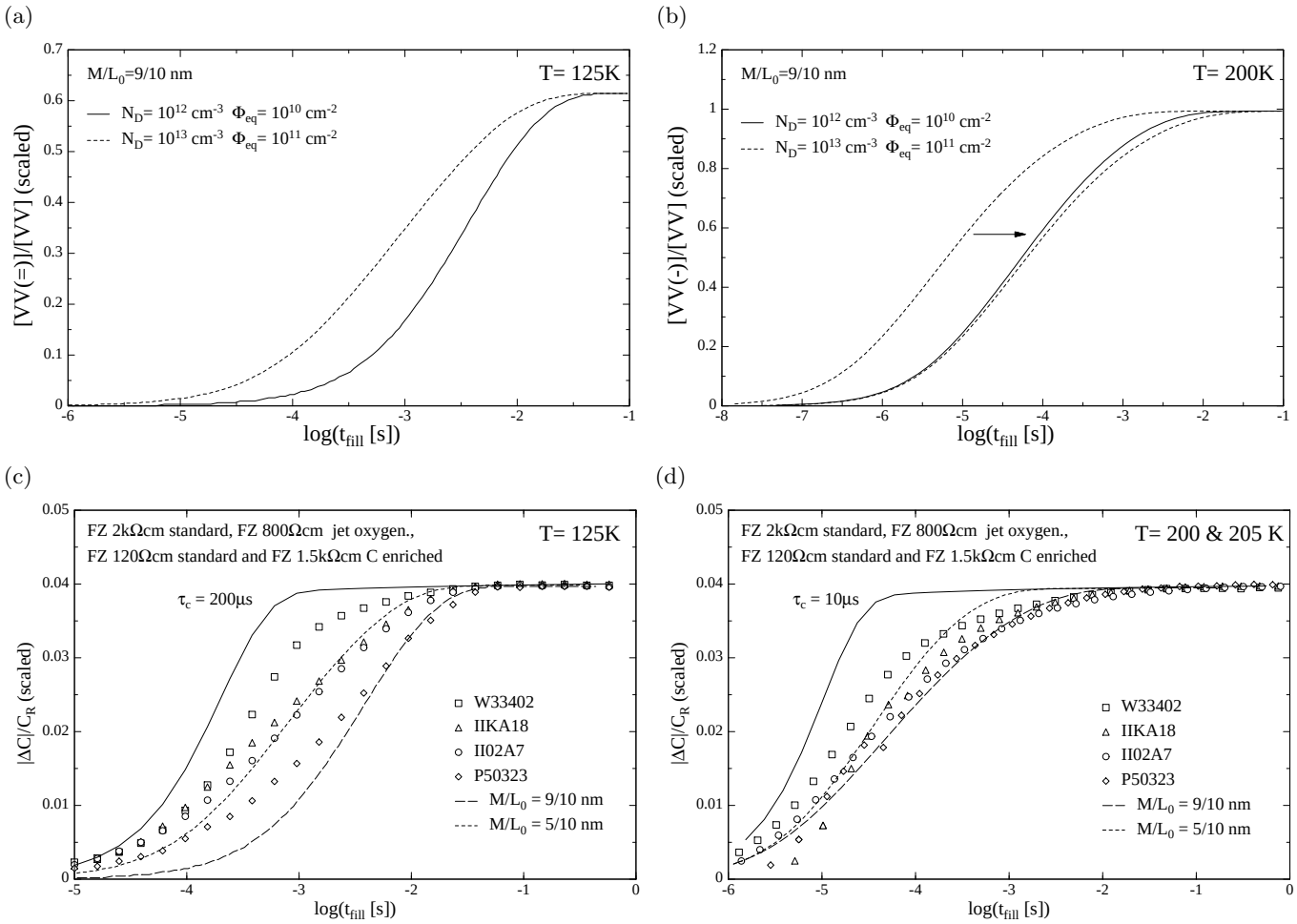

FIG. 3: The simulated capture characteristics of the processes (a) $VV(-/=)$ and (b) $VV(0/-)$ are presented. The measured capture characteristics of the processes (c) $VV(-/=)$ and (d) $VV(0/-)$ in various samples after particle irradiation are plotted (open symbols). The simulations of the capture characteristics (dashed lines) and the capture characteristics with a constant capture rate (solid line) are included. The capture time constant $\tau_c = 10\ \mu s$ is in the order of the time constant for the capture processes of a single divacancy $VV(-/=)$ and $VV(0/-)$. The capture characteristic with $\tau_c = 200\ \mu s$ is shown to guide the eye. The signals are scaled. For sample details see Table III.

TABLE III: The samples in which the electrical capture characteristics of the divacancy have been measured are listed.

Sample	Material type	N_D [cm^{-3}]	Particle type	Tempering	$[VV(=)]/[VV(-)]$
W33402	FZ 2kΩcm standard	2.26×10^{12}	10 MeV p^+	4min@80 °C	0.48
IIKA18	FZ 800Ωcm jet-oxyg.	6.00×10^{12}	192 MeV π^+	1280min@60 °C	0.42
II02A7	FZ 120Ωcm standard	3.73×10^{13}	Be(d,n) n	5470min@80 °C	0.44
P50323	FZ 1.5kΩcm C enrich.	3.18×10^{12}	Reactor n	80min@60 °C	0.14

dopant concentration is $N_D = 10^{12}$ cm^{-3}. A dependence of the capture rate on the number of divacancies in a cluster is apparent. The deviation from the capture characteristic with a constant capture rate diminishes with decreasing numbers of divacancies in a cluster.

In Fig. 3d the measured capture characteristics $VV(0/-)$ are shifted on the time scale with $\log(N_D/10^{12}\ \text{cm}^{-3})$ to take into account the different majority charge carrier concentrations under equilibrium conditions. This results in a good coincidence of the capture characteristics. A dependence on the impurity content, particle type and annealing state is hardly seen. The capture characteristics exhibit a large deviation from the capture characteristic with a constant capture rate ($\tau_c = 10\ \mu$s). In Fig. 3d the simulations of the capture characteristics are also depicted. The parameters are $M = \{5, 9\}$ and $L_0 = 10$ nm. The dopant concentration is $N_D = 10^{12}$ cm^{-3}. The capture rate is not constant and depends only weakly on the number of divacancies in a cluster. This dependence is consistent with

the experimental results. The deviation from the capture characteristic with a constant capture rate diminishes with decreasing numbers of divacancies.

VII. DISCUSSION

A. Impurity-defect shell build-up

The above simulation has shown that the number of divacancies in a cluster with a diameter of 20 nm is in the range from six to eleven for the various irradiation sources: 7-10 MeV protons, 27 MeV protons, 23 GeV protons, 192 MeV π^+-pions and Be(d,n) neutrons with a mean energy of 5.3 MeV. Thus the build-up of an impurity-defect shell[3,27,29] due to the migration of interstitial carbon atoms C_i towards the clusters is questionable, since the divacancies in the clusters are likely separated from each other by more than a few (2−3) lattice constants. Point defects such as C_i atoms are able to move through the outer cluster part without any reaction and hence a reaction in the inner cluster part becomes feasible. Moreover, the mobile C_i atoms are in the neutral charge state in n-type silicon under thermal equilibrium conditions at room temperature and hence no coulomb interaction exits. Only if the temperature is $T \leq 60$ K — at which the capture characteristic of C_i is measured[7,29] — a repulsive electric force between the single negatively charged C_i atoms and the double negatively charged divacancies occurs. Therefore, it is suggested that a repulsive force between the C_i atoms and hypothetical multi-interstitial defects, which cause a compression of the surrounding lattice, could prevent the penetration into the cluster core at room temperature.

It has already been postulated that a C_i atom causes a lattice compression and that a cluster of divacancies causes a lattice tension.[30] For both sources of deformation additional energy is stored in the lattice. A point defect, that causes a local lattice compression, placed in a tension field of an extended defect relaxes the lattice deformation in its neighborhood. Thus the amount of stored energy is reduced. An attractive force is induced between the point defect and the extended defect assuming the amount of gained relaxation energy increases as the distance between both defects decreases. On the other hand, it is concluded that two lattice compression fields in the vicinity of each other induce a repulsive force. One notes that the above model is strongly simplified and that the assignments of self-interstitial clusters in silicon to experimental data are ambiguous.[42] However, other experimental results seem to indicate that the lattice in the proximity of the divacancies is compressed.[10]

Eventually, one conjectures that inside the clusters the lattice is locally compressed due to interstitial defects and outside the clusters a tension field is created, because vacancy complexes prevail in the clusters. Consequently, the build-up of an impurity-defect shell due to the accumulation of C_i atoms around the clusters is still conceivable.[3,27,29] Furthermore, it is assumed that the defect density in the cluster envelope is small after low fluence irradiation used for the DLTS studies and hence the impurity-defect shell is transparent for other migrating defect species. A higher defect density augments the opacity of the impurity-defect shell.

B. Annealing of cluster damage

It has been found that the ratio $[VV(=)]/[VV(-)]$ decreases with increasing number of divacancies in a cluster, if the cluster diameter is kept constant. Therefore a decay of divacancies in the clusters is suggested during annealing at moderate temperatures $T < 80$ °C, since the ratio $[VV(=)]/[VV(-)]$ increases. It has previously been suggested that during the annealing of the cluster damage a dissociation of divacancies takes place.[7,10] An evaporation of vacancies is observed during the long-term annealing at $T = 60$ °C. Otherwise, the activation energies of the diffusion and dissociation processes of the divacancy are too high to allow a dissolution of a divacancy cluster at room temperature or moderate temperatures $T = 60-80$ °C. The elastic energy deposited into strain and deformation fields may be employed to break divacancies inside the cluster regions. Thus a dissociation of divacancies during annealing at room temperature is possible. Commonly, the relief of strain and deformation fields is associated with a restructuring of the cluster damage including decay and rearrangement of defects within the clusters. One speculates that the energy barrier for restructuring of cluster damage, which comprises the decay of divacancies and the relaxation of strain and deformation fields, is smaller than the energy barrier for dissociation of a single divacancy.

Another source of vacancies could be the dissociation of larger vacancy complexes, but a decay of higher-order vacancy complexes at room temperature can be excluded, since the vacancy aggregates V_3,...,V_6 are more stable than the divacancy.[43] The most stable complex is the hexagonal ring of vacancies V_6 which has eighteen metastable configurations with appreciable higher energies (> 0.8 eV). The gained energy from rearrangement to a stable configuration of V_6 can also be employed to dissociate other nearby defect complexes such as divacancies. The time scale, on which the rearrangement to the stable configuration at room temperature takes place, is not known. At high temperature T

= 1200 K the rearrangement is assumed to be completed on the picosecond time scale.[43] Otherwise, it is not known, if higher-order vacancy complexes such as V_6 are generated during high energy particle irradiation at room temperature.

Besides, silicon multi-interstitials are able to annihilate with divacancies in the cluster regions. Furthermore, it is remarkable that a reduction of divacancies could also be due to a rearrangement into higher-order vacancy complexes. A possible candidate is the hexagonal ring V_6 which has a shallow acceptor level at $E_C - 0.04$ eV.[44] Thus it is not detectable with the DLTS method. These two processes have already been introduced in Ref. 30. The former one occurs in the temperature range $T = 150{-}200$ °C. The latter one begins at a temperature $T > 250$ °C,[45] at which as well the dissociation of single divacancies starts.[16,46] For this case, one assumes the movement of vacancies to be constrained to the cluster regions.

To summarize, the annealing of divacancies accompanied by an evaporation of vacancies takes place in the outer part of the clusters and the feasible coalescence into multi-vacancy complexes in the inner part of the clusters, because the mean distance between decaying divacancies in the cluster core is less than the capture radius for formation of multi-vacancy complexes.[31] The hypothetical annihilation of divacancies with nearby silicon multi-interstitials I_n is thought to occur in the interior of the clusters. The annealing process may be accompanied by a release of vacancies for the reaction $I + VV \rightarrow V$ and of interstitial clusters I_{n-2} for the reaction $I_n + VV \rightarrow I_{n-2}$ with $n \geq 2$.

VIII. SUMMARY AND CONCLUSIONS

It is demonstrated that the results of DLTS measurements obtained from high resistivity n-type silicon samples after particle irradiation can be explained by a model of a Gaussian distribution of divacancies in the clusters. The ratio $[VV(=)]/[VV(-)]$ decreases with increasing line density M/L_0 (M is the number of divacancies in a cluster and L_0 the characteristic width of the Gaussian distribution).

For $L_0 = 10$ nm the numbers of divacancies are M=6−8 for 7-10 MeV proton irradiation, M=7−9 for 27 MeV proton irradiation, M=8−10 for 23 GeV proton/192 MeV π^+-pion irradiation and M=10−11 for Be(d,n) neutron irradiation. The mean energy of the Be(d,n) neutrons is 5.3 MeV. It should be mentioned that the number of divacancies in a cluster is too low for the vindication of a continuous density distribution function.

The measured capture characteristics of the negative charge states of the divacancy $VV(-/=)$ and $VV(0/-)$ are described reasonably by the simulated capture characteristics. The observed dependence of the capture characteristic $VV(-/=)$ on the annealing state is consistent with the theory, likewise the weak dependence on the annealing state and the dependence on the dopant concentration of the capture characteristic $VV(0/-)$. The reduced capture rates suggest the electron concentration in n-type silicon to be diminished due to negatively charged divacancies in the cluster regions. This effect is more conspicuous at low temperatures, since all divacancies are already in the single negative charge state at the beginning of the capture process $VV(-/=)$. The bending of the electronic band structure is determined by the distribution of charged divacancies in the cluster regions. The model of a Gaussian density distribution seem to be reasonable.

The build-up of an impurity-defect shell due to the migration of interstitial carbon atoms C_i towards the clusters has been discussed. Lattice strain and deformation fields are thought to be responsible for the interaction between the point defect C_i and the extended cluster defect. It is conjectured that inside the clusters the lattice is locally compressed due to interstitial defects and outside the clusters a tension field is created, because vacancy complexes prevail in the clusters.

The dissociation of divacancies in the clusters during annealing at moderate temperatures $T < 355$ K has been suggested. The increase of the ratio $[VV(=)]/[VV(-)]$ observed during annealing substantiates the decay of divacancies. Different annealing mechanism for the dissociation of divacancies has been discussed. Moreover, one assumes that a dissociation of divacancies takes place in the outer part of the clusters and a feasible coalescence into multi-vacancy complexes in the inner part of the clusters. Also the annihilation of divacancies with nearby interstitial clusters is suggested.

IX. ACKNOWLEDGEMENTS

I would like to thank K. Zankel for initiating this work. Support from the European Commission contract No. ERB-FMRX-CT-980208 is greatly appreciated. The diodes were provided by the CERN RD48 Collaboration.

[1] M. Moll, H. Feick, E. Fretwurst, G. Lindstroem and C. Schuetze, Nucl. Instr. Meth. Phys. Res. A **388**, 335 (1997).

[2] V.A.J. van Lint, R.E. Leadon and J.F. Colwell, IEEE Trans. Nucl. Sci. **19**, 181 (1972).
[3] M. Kuhnke, E. Fretwurst and G. Lindstroem, Nucl. Instr. Meth. Phys. Res. B **186**, 144 (2002).
[4] M. Huhtinen, Technical Note ROSE/TN/2001-02, CERN, 2001.
[5] K. Nordlund, Nucl. Instr. Meth. Phys. Res. B **188**, 41 (2002).
[6] K. Nordlund, M. Ghaly, R.S. Averback, M. Caturla, T. Diaz de la Rubia and J. Tarus, Phys. Rev. B **57**, 7556 (1998).
[7] M. Kuhnke, *Microscopic Investigations on Various Silicon Materials Irradiated with Different Particles with the DLTS Method*, Ph.D. thesis, DESY-Thesis-2001-009, University of Hamburg, 2001.
[8] M. Moll, E. Fretwurst, M. Kuhnke and G. Lindstroem, Nucl. Instr. Meth. Phys. Res. B **186**, 100 (2002).
[9] M. Moll, *Radiation Damage in Silicon Particle Detectors*, Ph.D. thesis, DESY-Thesis-1999-040, University of Hamburg, 1999.
[10] M. Kuhnke, IEEE Trans. Nucl. Sci. **49**, 2599 (2002).
[11] K. Nordlund, P. Partyka, Y. Zhong, I.K. Robinson, R.S. Averback, P. Ehrhart, Nucl. Instr. Meth. Phys. Res. B **147**, 399 (1999).
[12] L.C. Kimerling, IEEE Trans. Nucl. Sci. **23**, 1497 (1976).
[13] B.G. Svensson, B. Mohadjeri, A. Hallén, J.H. Svensson and J.W. Corbett, Phys. Rev. B **43**, 2292 (1991).
[14] A.V. Vasil'ev, S.A. Smagulova and S.S. Shaĭmeev, Sov. Phys. Semicond. **16**, 1279 (1982).
[15] B.G. Svensson, C. Jagadish, A. Hallén and J. Lalita, Phys. Rev. B **55**, 10498 (1997).
[16] G.D. Watkins and J.W. Corbett, Phys. Rev. **138**, A543 (1965).
[17] The concentration of ion-induced vacancies was obtained from TRIM calculations (Version 90.05) assuming a displacement threshold energy of 13 eV in Ref. 15.
[18] S.K. Estreicher, M. Gharaibeh, P.A. Fedders and Pablo Ordejón, Phys. Rev. Lett. **86**, 1247 (2001).
[19] P. Partyka, Y. Zhong, K. Nordlund, R.S. Averback, I.M. Robinson and P. Ehrhart, Phys. Rev. B **64**, 235207 (2001).
[20] M. Gharaibeh, S.K. Estreicher, P.A. Fedders, Physica B **308-310**, 510 (2001).
[21] L.M. Howe and M.H. Rainville, Nucl. Instr. Meth. Phys. Res. B **19/20**, 61 (1987).
[22] M.O. Ruault, J. Chaumont and H. Bernas, Nucl. Instr. Meth. Phys. Res. **209/210**, 351 (1983).
[23] N.G. Goleminov, E.A. Kramer-Ageev and Yu.A. Mironov, Phys. Status Solidi (a) **28**, 371 (1975).
[24] A.V. Vasil'ev, L.S. Smirnov and S.S. Shaĭmeev, Sov. Phys. Semicond. **20**, 465 (1986).
[25] V.F. Zinchenko and Yu.V. Karpik, Sov. Phys. Tech. Phys. **27**, 990 (1982).
[26] I.V. Antonova, A.V. Vasil'ev, V.I. Panov and S.S. Shaĭmeev, Sov. Phys. Semicond. **23**, 944 (1989).
[27] A.V. Vasil'ev, S.A. Smagulova and S.S. Shaĭmeev, Sov. Phys. Semicond. **16**, 84 (1982).
[28] I.V. Antonova, A.V. Vasil'ev, V.I. Panov and S.S. Shaĭmeev, Sov. Phys. Semicond. **23**, 671 (1989).
[29] M. Kuhnke, E. Fretwurst and G. Lindstroem, Nucl. Instr. Meth. Phys. Res. A **485**, 140 (2002).
[30] V.I. Kuznetsov, P.F. Lugakov and V.V. Shusha, Rad. Effects Lett. **86**, 199 (1984).
[31] A. Bongiorno and L. Colombo, Phys. Rev. B **57**, 8767 (1998).
[32] B.R. Gossik, J. Appl. Phys. **30**, 1214 (1959).
[33] G. Lindström, M. Moll and E. Fretwurst, Nucl. Instr. Meth. Phys. Res. A **426**, 1 (1999).
[34] W. Shockley and J.T. Last, Phys. Rev. **107**, 392 (1957).
[35] M.A. Green, J. Appl. Phys. **67**, 2944 (1990).
[36] The fit of the experimental data from Ref. 37 in H. Feick, Ph.D. thesis, DESY F35D-97-08, University of Hamburg, 1997, Appendix A, p. 181.
[37] C. Canali, G. Ottariani, A. Alberigi Quaranta, J. Phys. Chem. Solids **32**, 1707 (1971).
[38] S.M. Sze, *Semiconductor Devices Physics and Technology* (John Wiley & Sons, New York, 1985), Chap. 6, p. 239.
[39] K. Gill, G. Hall and B. MacEvoy, J. Appl. Phys. **82**, 126 (1997); *ibid.* **85**, 7990 (1999).
[40] M. Kuhnke *et al.*, 6^{th} ROSE Workshop RD48, CERN, 2000.
[41] D. Pons, J. Appl. Phys. **55**, 3644 (1984).
[42] R. Jones, T.A.G. Eberlein, N. Pinho, B.J. Coomer, J.P. Goss, P.R. Briddon and S. Öberg, Nucl. Instr. Meth. Phys. Res. B **186**, 10 (2002).
[43] J.L. Hastings, S.K. Estreicher and P.A. Fedders, Phys. Rev. B **56**, 10215 (1997).
[44] B. Hourahine, R. Jones, A.N. Safonov, S. Öberg, P.R. Briddon and S.K. Estreicher, Phys. Rev. B **61**, 12594 (2000).
[45] L.S. Berman, V.B. Voronkov, V.A. Kozlov and A.D. Remenyuk, Sov. Phys. Semicond. **26**, 847 (1992).
[46] G.D. Watkins, Proceedings of the 1^{st} ENDEASD Workshop, Santorini, Greece, 1999.